22nd International Conference on Renewable Energies and Power Quality
(ICREPQ'24) Bilbao (Spain), 26th to 28th June 2024
Renewable Energy and Power Quality Journal (RE&PQJ)
ISSN 2172-038 X, Volume No.22, September 2024

Fault detection and mitigation in MVDC grids using a Non-Unit Voltage Ratio Derivative Algorithm

A. Blazquez[1], M.J. Pérez-Molina[2], P. Eguia[1], D.M. Larruskain[1], A. Iturregi[1], E. Torres[1]

[1] Department of Electrical Engineering, Faculty of Engineering of Bilbao, Universidad del País Vasco UPV/EHU
Alameda Urquijo s/n, 48013 Bilbao (Spain)
Phone/Fax number: +0034 946 014970

[2] Oceanic Platform of the Canary Islands (PLOCAN), Carretera de Taliarte s/n (Lighthouse), 35214, Telde, Spain

Abstract. Future MVDC grids will be used to reinforce the grid infrastructure enhancing transmission capabilities, minimizing losses, and providing capability to compensate reactive power as well as to control load flows. This paper addresses the protection of MVDC grids, which is one of the main challenges to be overcome, before taking advantage of all the inherent benefits that this technology will bring. The main objective of this paper is to validate a non-unit voltage derivative fault detection algorithm in a MVDC grid with green hydrogen production. The performance is analyzed with different fault cases and fault locations. As a main conclusion, the distance is the most relevant factor, which affects detection and tripping times.

Key words. Algorithm, fault detection, fault mitigation, green hydrogen, non-unit, MVDC grid, voltage derivative.

1. Introduction

Currently, there is a small number of Medium Voltage Direct Current (MVDC) systems around the world. Basically, they consist of motor drive system applications, including ships and aircrafts [1]. Besides, regarding the application in power systems, just a small number of installations have been commissioned in recent years. One project in UK, ±27 kV Angle-DC [2] and a few in China: Jiangdong ±10 kV three-terminal project [3], Zhuhai Tangjia Bay Project [4], Zhangbei ±10 kV three-terminal project [5] and Suzhou ± 20 kV four-terminal project [6].

The integration of MVDC systems in the power system is still at the initial stage, thus it is required to overcome a number of challenges, such as the development of control and protection systems, switchgear and standards [1], [7]. This paper deals with the protection of MVDC grids.

Due to the small resistance of DC links, DC faults produce a sharp collapse in the voltage and a fast increase in the current up to very high values. These characteristics present a challenge for the development of DC protection systems since power electronics can only withstand twice their nominal current. Therefore, the protection system must detect and clear faults in the range of less than 10 ms, and, thus, highly fast and selective fault detection algorithms need to be developed.

There is a vast number of fault detection and location algorithms proposed for high Voltage Direct Current (HVDC) systems. Nevertheless, the performance of those algorithms has only been validated in HVDC systems and may not be feasible for MVDC systems, as there could be limitations in the correct performance. Besides, in the literature, few publications address the protection scheme or fault detection and location algorithms for MVDC systems. In this regard, authors of [8] propose a protection scheme for the shipboard electrical system of a multiterminal MVDC grid, based on the overcurrent principle. A protection system is applied to a MVDC microgrid in [9], authors introduce the protection of a MVDC microgrid, based on differential and overcurrent algorithms. Reference [10] proposes a protection method based on current derivatives and the fluctuating pattern of the current. The protection scheme in [11] detects faults according to the current and voltage magnitudes. Paper [12] proposes a current differential detection method for MVDC distribution networks wavelet transform.

In the presented work, a non-unit voltage derivative based fault detection algorithm for HVDC grids [13] will be adapted to a MVDC grid and validated in a system with renewable energy sources and electrolyzers.

The paper is structured in the following way; section 2 describes the fault detection algorithm, section 3 exposes the different study cases validated with simulations and in section 4 are described the main conclusions of the study carried out.

2. Non-unit voltage ratio derivative fault detection algorithm

The non-unit voltage ratio derivative fault detection algorithm is based on measuring the DC voltage [13]. More precisely, it is performed by measuring the voltage at both sides of the limiting inductor placed in the DC lines, as it can be seen in Figure 1.
In steady state, under no fault condition, the inductor acts as a short-circuit and the measured voltages at both sides are equal. However, when a fault occurs, the measured voltages at both sides of the inductor will not be the same, due to damping characteristic of limiting inductors. The

voltage difference across the inductor ($V_{inductor}$) is defined in equation (1).

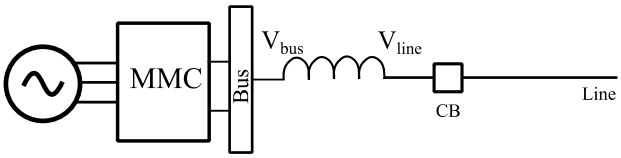

Fig.1. Voltage measurement of the inductor

$$V_{inductor} = L \cdot \frac{di}{dt} = V_{bus} - V_{line} \quad (1)$$

Where Vbus is the voltage measured at the bus side of the limiting inductor and Vline is the voltage measured at the DC line side.

The proposed algorithm is the combination of two calculations based on local voltage measurements. The concurrent operation of these two calculations improves the selectivity of the proposed algorithm by avoiding nuisance operation due to misdetection of normal operation transients or oscillations as faults.

First, the Voltage Ratio (VR) of the voltages at both sides of the limiting inductor is calculated as in (2). In normal operation, as the two voltages are equal, this value is one or very close to one

$$\boldsymbol{VR = \frac{V_{line}}{V_{bus}}} \quad (2)$$

Afterwards, the derivative of the voltage ratio is calculated. It consists on taking two consecutive VR samples and applying equation (3).

$$VRD = \frac{dVR}{dt} = \frac{VR_{t_2} - VR_{t_1}}{t_2 - t_1} \quad (3)$$

Where, VR_{t2} is the VR calculated corresponding to the time t_2 and VR_{t1} the one corresponding to the time t_1.

The subtraction of the divisor always will have as a result the sample time used to perform the algorithm, so t_2 always will be greater than t_1. As it has been aforementioned, in steady state and without a fault condition, VR is equal to one, so the Voltage-Ratio-Derivative (VRD) is equal to zero or very close to zero due to the oscillating nature of the system and precision error in measurements.

Moreover, the proposed protection scheme provides directionality since it is capable of differentiate between forward and backward faults and, therefore, it allows fault discrimination between bus and line faults.

When a line fault happen, V_{line} collapses to a lower value than V_{bus}, so the calculated VR is less than 1, and, consequently, VRD presents a negative value.

$$Line\ Fault: V_{bus} > V_{line} \Longrightarrow VR < 1 \Longrightarrow VRD < 0 \quad (4)$$

Conversely, V_{bus} presents a lower value than V_{line} during a bus fault. Then, VR and VRD present a value greater than 1 and a positive value, respectively.

$$Bus\ Fault: V_{bus} < V_{line} \Longrightarrow VR > 1 \Longrightarrow VRD > 0 \quad (5)$$

By comparing the calculated VR and VRD to pre-determined threshold values fault detection and discrimination can be achieved. In case both parameters overcome their thresholds, a fault condition is detected, if not a transient has been detected, so the system remains under normal operation and the algorithm starts calculating again.

The following equations show fault detection and discrimination criteria:

$$Line\ Fault: \begin{cases} VR < THR_1 \\ VRD < THR_3 \end{cases} \quad (6)$$

$$Bus\ Fault: \begin{cases} VR > THR_2 \\ VRD > THR_4 \end{cases} \quad (7)$$

where THR_1 takes a value between 0 and 1 and THR_2 takes a value higher than 1; and THR_3 takes a negative value and THR_4 is a positive value.

The proposed algorithm follows the steps shown in Figure 2 to achieve fault detection.

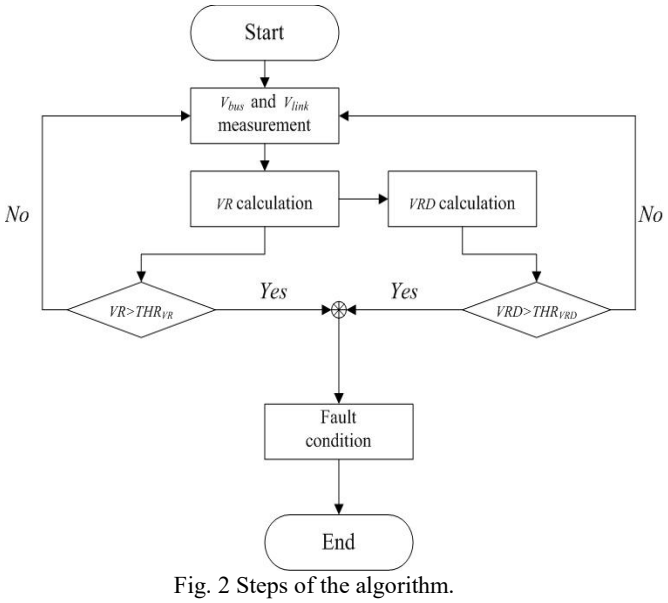

Fig. 2 Steps of the algorithm.

3. Study case

In Figure 3, the proposed MVDC grid can be seen, which has been used to validate the non-unit voltage ratio derivative algorithm using the software PSCAD/EMTDC. The used MVDC grid, is an scaled version of the HVDC grid defined in [14], which uses DC circuit breakers, due to its feasibility and speediness.

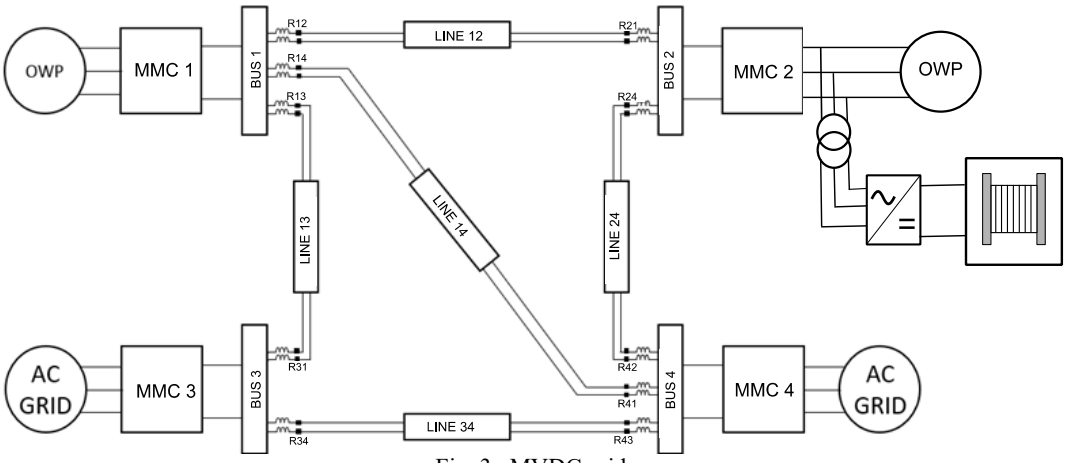

Fig. 3. MVDC grid.

The MVDC grid is made up of four Modular Multilevel Converters(MMC), with the rated powers shown in Table I.

Table I.-Rated power of MMCs

MMC	Rated Power
1	80 MVA
2	80 MVA
3	75MVA
4	85MVA

MMC1 and MMC2 are connected to an onshore wind power station at their AC side, while MMC3 and MMC4 are connected to AC grids. MMC2 has an electrolyzer connected through a transformer and a rectifier. The DC side is a meshed grid which interconnects the four converters through five DC lines, with different lengths, (Table II)

Table II.- Length of DC lines.

DC Line	Length
L12	2 km
L13	60 km
L14	15 km
L24	12 km
L34	50 km

AC grids voltage is 36 kV, while DC side voltage is ±25 kVdc. As it is shown in Figure 3, at the end of each DC line, in both positive and negative poles, there is a 100 mH inductor connected in series with a DC hybrid circuit breaker. Since it is a meshed grid, a full selective strategy is considered, in such a way that in case a fault condition exists, the algorithm is able to isolate the zone under fault condition, and allows the rest of the system to work in normal operation. The proposed system is tested using a sampling frequency of 200 kHz, resulting in a sample time of 5µs, since it is a value in the range of those commonly found in the literature [15]. The PEM electrolyzer connected to MMC2 operates at 450Vdc. The power transformer connected to the AC side, provides galvanic isolation to the electrolyzer and the rectifier converts the AC voltage into DC voltage at the required level.

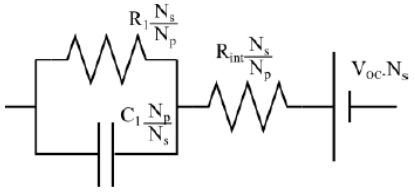

Fig.4. Equivalent circuit of the electrolyzer [16].

The equivalent circuit of the electrolyzer shown in Figure 4, consists on 70 cells in series and 275 strings in parallel [16]. It works as a DC load, consuming 1 MW.

In this section, the analysed study cases with different type of faults, fault locations and fault resistances will be shown, as well as an initial steady state simulation scenario.

A. Steady state

In this first scenario, the normal operation of the system is shown. Afterwards, this scenario will be compared with the different fault scenarios. The analyzed fault scenarios are located at Bus 2 and DC Line 24, so graphics of VR and VRD the correspondent relays will be shown.

In steady state, the DC current shown in Figure 5 is stable and continuous. In figure 6, VR and VRD are visualized in steady state. As it has been mentioned before, VR and VRD correspond to their steady state values, one and zero respectively. All the fault scenarios occur for t=6.5s.

.

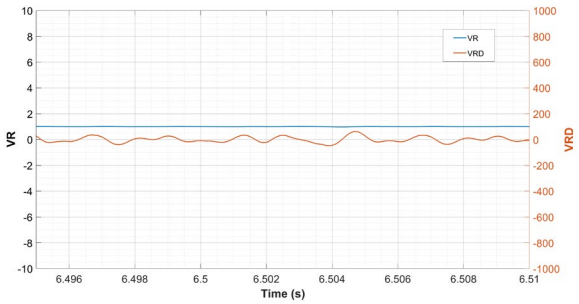

Fig. 6 VR and VRD in steady state.

B. *Faults at DC bus 2*

a. Pole-to-pole solid fault at DC bus 2

The first fault scenario in the proposed MVDC grid, a pole-to-pole fault at DC bus 2. The fault resistance is 0.01 Ω, which is the lowest fault resistance (R_f) used in the simulations. For busbar faults, the selected thresholds are 2 for VR and 200 for VRD.

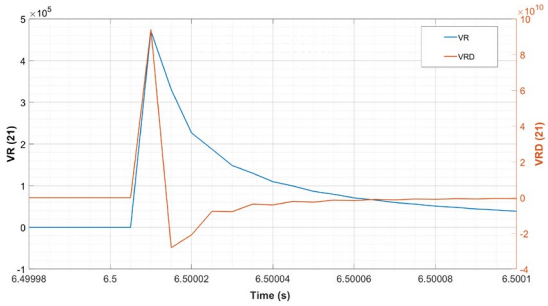

Fig. 7. P2P fault in DC bus 2 R_f=0.01Ω R 21.

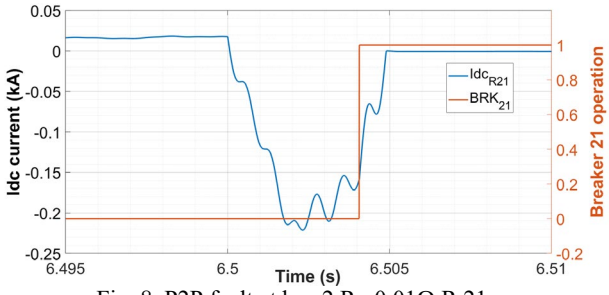

Fig. 8. P2P fault at bus 2 R_f=0.01Ω R 21.

Figure 7 shows VR and VRD measured at relay R 21, while Figure 9 shows the same indicators measured at R 24. Analysing Figure 7, VR and VRD exceed their respective threshold in 10 µs. Figure 7 and figure 9, are almost equal because as the fault is occurring inside the bus, both relays, R 21 and R 24, are assumed to have the same distance to the fault. VR and VRD reach very high values due to the low resistance of the fault and the quick bus voltage drop.

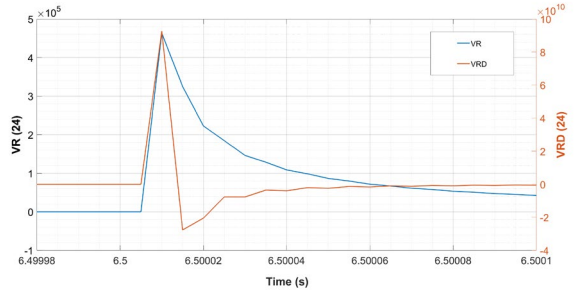

Fig. 9. P2P fault at bus 2 R_f=0.01Ω R 24.

Regarding to Figures 8 and 10, it can be seen the maximum DC current in each relay, R 21 and R 24, and the time when the breaker operates, bringing the fault current to zero. For this case, both breakers operate at the same time, 4.065 ms, mitigating the fault.

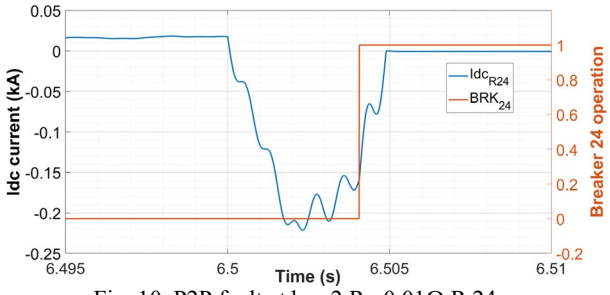

Fig. 10. P2P fault at bus 2 R_f=0.01Ω R 24.

b. Pole-to-ground 2 Ω fault at DC bus 2

Figure 11 and Figure 12, analyse a pole-to-ground fault at bus 2, with a fault resistance of 2Ω, measured at relay R 21 and R 24, respectively. As the fault resistance has been considerably increased, the value of VR in the detection time is much lower than in the previous case. Nevertheless, VRD continues being very high, since it is the derivative with respect to time. The increase of the fault resistance does not affect the detection time with the selected thresholds. Bus voltage drop is slower, but VR and VRD cross their thresholds both of them in 10 µs. In the bus faults, both pole-to-pole and pole-to-ground, VR and VRD are positive because the voltage which drops instantaneously is the bus voltage and not the line voltage. As the bus voltage is the divisor, it increases enormously the voltage ratio. This is the reason for selecting a threshold higher than one in busbar faults, according to equation (2), when a fault occurs the voltage ratio will be higher than one.

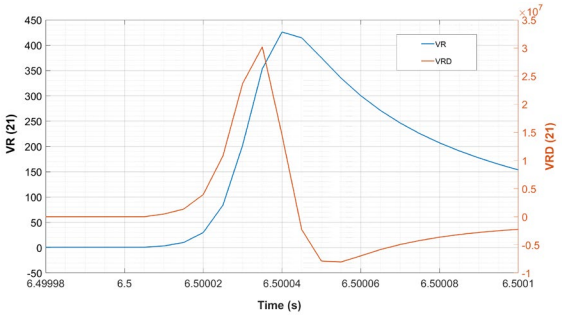

Fig. 11. P2G fault in DC bus 2 R_f=2Ω R 21.

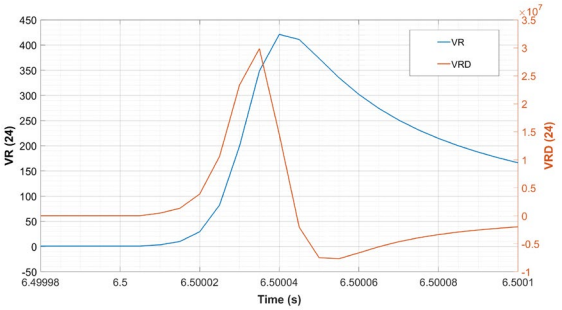

Fig. 12. P2G fault in DC bus 2 R_f=2Ω R 24.

Figure 13 and Figure 14, show the maximum DC currents reached during the fault and the breakers BRK21 and BRK24 operation to mitigate the fault. As it can be seen, they manage to interrupt the fault in 2.455 ms, even faster than for the pole to pole fault in the bus 2.

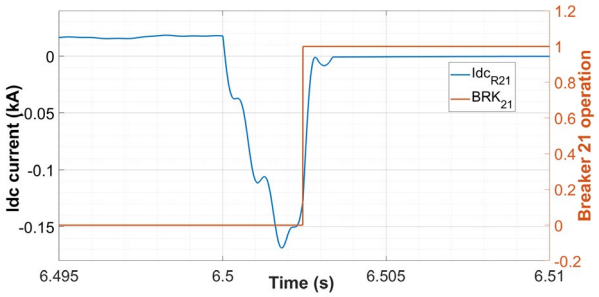

Fig. **13**. P2G fault in DC bus 2 R_f=2Ω R 21.

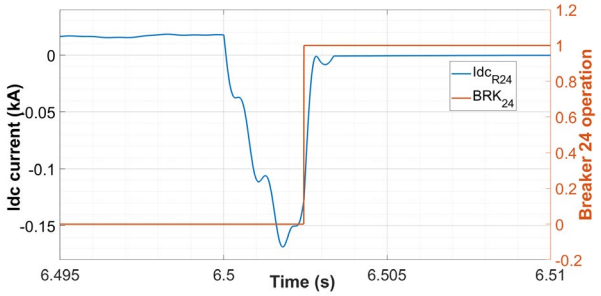

Fig. 1**4**. P2G fault in DC bus 2 R_f=2Ω R 24.

C. Faults in DC line 24

To continue with the fault analysis in the MVDC grid, different faults have been simulated in DC line 24, which is 12 km long. The determined thresholds for the line faults are 0,90 for VR and -1500 for VRD.

a. Pole-to-pole 20 Ω *fault in line 24*

In this first line fault scenario, the pole-to-pole fault is located at the beginning of line 24. It means that the fault is located just next to relay R 24 and consequently, it is twelve kilometres away from the relay R 42. The fault resistance for this case, 20 Ω, is the highest one considered in the simulations. The distance, as well as the fault resistance have a big impact in the fault detection time.

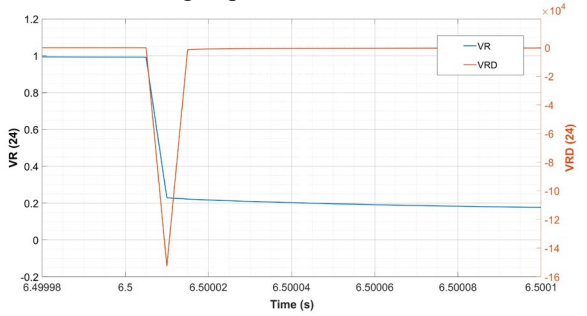

Fig. 15. P2P fault in DC line 24 R_f=20Ω 0% R 24.

Figure 15 shows, how relay R 24, the one which is closer to the fault, detects the fault in 10 µs, while in figure 16, relay R 42 needs 65 µs to detect that fault. In the line fault, unlike the bus fault, VR and VRD fall to negative values. The reason is that in line faults, the line voltage drops instantaneously instead of bus voltage, so in case a fault occurs the voltage ratio calculated will be less than one. That is the reason why the selected threshold for VR is below one in line faults and for VRD it is negative.

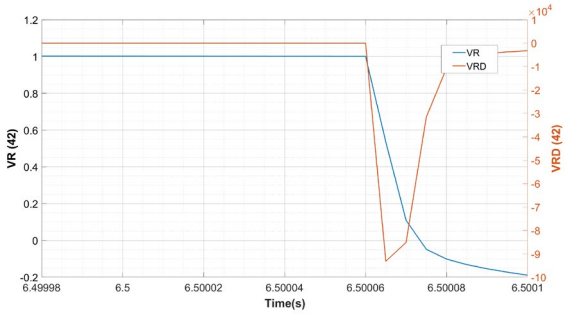

Fig. 16. P2P fault in DC line 24 R_f=20Ω 0% R 42.

Figure 17 and Figure 18 show the current interruption time, when the breakers operate to mitigate the fault through the line 24, and the maximun currents reached.

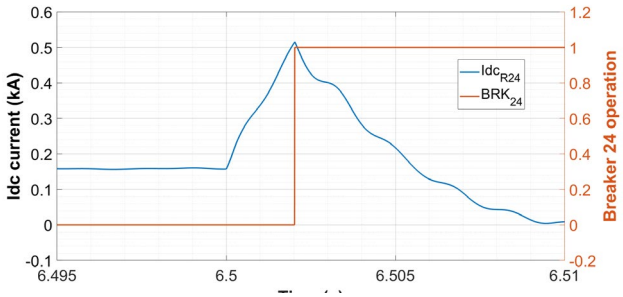

Fig. 17. P2P fault in DC line 24 R_f=20Ω 0% R 24.

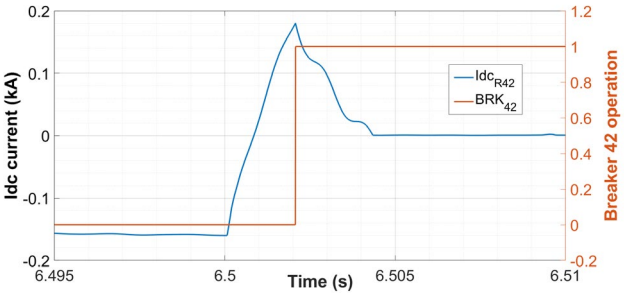

Fig. 18. P2P fault in DC line 24 R_f=20Ω 0% R 42.

Breaker BRK21 interrupts the current in 2.025 ms and BRK24 in 2.075ms. This minor difference is because the fault location and can be seen in the fault detection times. As it is in the 0% of the line, close to the relay R 24, the fault is detected faster.

b. Pole-to-ground solid fault in line 24

Figure 19 and Figure 20 show the last fault case. It is a pole-to-ground fault located in the middle of line 24, so it is six km from each relay (R 24 and R 42). In both graphics, VR and VRD overtake their thresholds in 40 µs and 35 µs, respectively. This time, the fault resistance is 0.01 Ω, as in the first bus fault case. Despite the two cases are different, because of the fault location and fault type, here the factor, which makes the main difference, is the distance to the fault. Six kilometres is enough to see a considerable delay in the fault detection time.

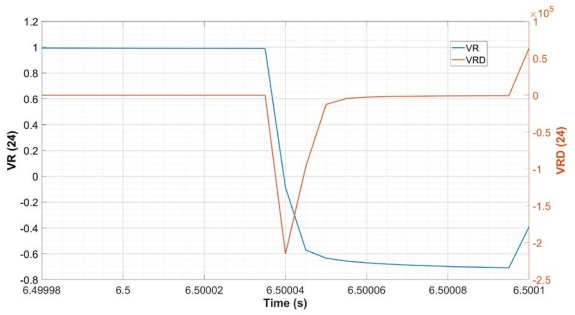

Fig.19. P2G fault in DC line 24 R_f=0.01Ω 50% R 24.

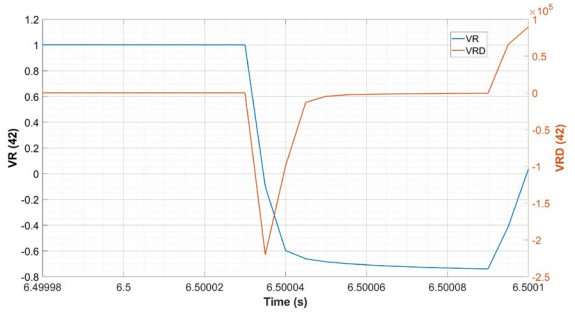

Fig. 20. P2G fault in midpoint of line 24, R_f=0.01Ω R 42.

Figure 21 and Figure 22, show the breakers operations, BRK24 and BRK42 respectively, and the peak currents during the fault. As it can be observed, the fault is interrupted in 2.055ms for BRK24 and 2.045 for BRK42.

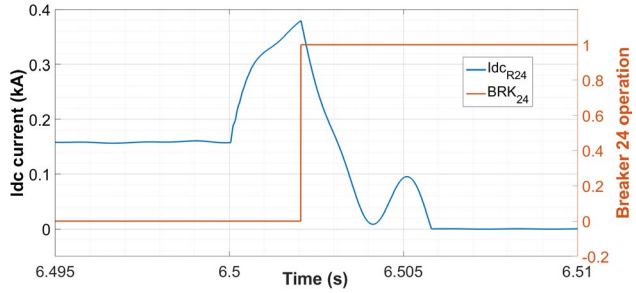

Fig.20. P2G fault in DC line 24 R_f=0.01Ω 50% R 24.

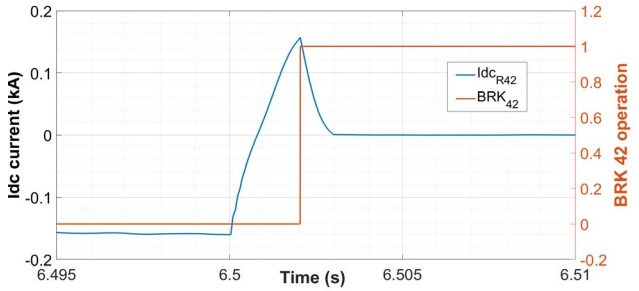

Fig. 21. P2G fault in midpoint of line 24, Rf=0.01Ω R 42.

In order to highlight and compare the obtained results of the considered scenarios, table III includes the detection times for all fault cases and table IIII the tripping times.

Table III, summarizes the obtained results of the fault detection time analysis. It can be seen that the biggest determining factor in terms of detection time, is the distance to the fault. As it can be seen in Table III, relays R 21 and R 42 have a no trip (NT) signal, when the fault is out of their area of protection. This is correct due to the selectivity of the algorithm.

Table III.- Fault detection times

Fault location	**DC Fault type**	**Rf (Ω)**	**R21 (µs)**	**R24 (µs)**	**R42 (µs)**
Bus 2	PtP	0.01	10	10	NT
Bus 2	PtG	2	10	10	NT
Line 24 0%	PtP	20	NT	10	65
Line 24 50%	PtG	0.01	NT	40	35

On the other hand, table IIII summarizes the obtained results of the breaker operation time analysis.

Fault location	**DC Fault type**	**Rf (Ω)**	**R21 (ms)**	**R24 (ms)**	**R42 (ms)**
Bus 2	PtP	0.01	4.065	4.065	NT
Bus 2	PtG	2	2.455	2.455	NT
Line 24 0%	PtP	20	NT	2.025	2.075
Line 24 50%	PtG	0.01	NT	2.055	2.045

4. Conclusion

This paper analyses a non-unit voltage ratio derivative algorithm, for a MVDC grid with renewable energy sources (RES) and an electrolyzer.

The proposed algorithm provides directionality and improved selectivity while fulfilling the restraining speed requirement of MVDC systems.

Different type of faults (pole-to-pole and pole-to-ground), with different fault resistances (0.01Ω, 2 Ω and 20 Ω) and locations have been simulated in PSCAD/EMTDC software, in order to determine the effectiveness of the algorithm.

Two different case studies have been analysed, a bus fault and a DC line fault. For each case study, two different scenarios have been analysed, a pole-to-pole fault and a pole-to-ground fault. In each scenario, voltage ratio and voltage ratio derivative of the two closest relays have been monitored, to determine the fault detection time for each case. As a conclusion, it can be said that the proper performance of the non-unit voltage-ratio-derivative algorithm has been successfully demonstrated. The proposed protection scheme meets the main DC protection requirements, such as speed, selectivity and reliability. Depending on the distance to the fault mainly, it takes more time to detect the fault, but not more than a few tens of microseconds. The combination of two algorithms (VR and VRD), makes it more feasible.

As future research work, the proposed algorithm will be compared with other algorithms under the same fault

conditions in a MVDC grid. Afterwards, the algorithms will be tested in a hardware in the loop platform.

Acknowledgement

The authors gratefully acknowledge the support from the Basque Government (GISEL research group IT1522-22 and Elkartek KK-2022/00039) and) and European Union – Next Generation EU (INVESTIGO program).

References

[1] WG C6/B4.37 Cigre, Medium voltage DC distribution systems, Ref. 875, July 2022.
[2] ANGLE-DC, 2015 Electricity Network Innovation Competition, Ofgem. Available: https://www.ofgem.gov.uk/ofgem-publications/97841/anglesubmission-pdf, accessed 14-02-2024.
[3] NR's MVDC Solution, ±10kV JiangDong MVDC for optimizing distribution network. Available: https://www.nrec.com/en/web/upload/2019/05/14/1557822630997rxt25.pdf, Accesed on 14-02-2024.
[4] L. Qu, et al., "Planning and analysis of the demonstration project of the MVDC distribution network in Zhuhai", Frontiers in Energy, vol. 13, pp. 120-130, 2019.
[5] X. Wang, R. Chen, J. Ge, T. Cao, F. Wang and X. Mo, "Application of AC/DC Distribution Network Technology Based on Flexible Substation in Regional Energy Internet," 2019 IEEE Innovative Smart Grid Technologies - Asia (ISGT Asia), Chengdu, China, 2019, pp. 4340-4345.
[6] C. Liang, J. Mengmeng, H. Qiang, Y. Xiaodong and L. Fei, "Engineering Simulation Analysis and Demonstration Application of Multi-terminal DC Distribution System," 2018 International Conference on Power System Technology (POWERCON), Guangzhou, 2018, pp. 2343-2349.
[7] A. Giannakis and D. Peftitsis, "MVDC Distribution Grids and Potential Applications: Future Trends and Protection Challenges," 2018 20th European Conference on Power Electronics and Applications (EPE'18 ECCE Europe), Riga, Latvia, 2018, pp. 1-9.
[8] M.E. Baran, N.R. Mahajan, "Overcurrent Protection on Voltage-Source-Converter-Based Multiterminal DC Distribution Systems" IEEE Transactions on Power Delivery, Vol. 22, No. 1, 2007.
[9] C. Yuan, M.A. Haj-ahmed, M.S. Illindala, Protection "Strategies for Medium-Voltage Direct-Current Microgrid at a Remote Area Mine Site", IEEE Transactions on Industry Applications, Vol. 51, No. 4, 2015.
[10] A. Kassem, H. Sabra, A.A. Ali1, K.M. Abdel-Latif, "Setting-Less Protection Technique for Mvdc Networks" Available: http://dx.doi.org/10.2139/ssrn.4446693, accessed 14-02-2024.[11] Z. Dai, H. Zhu, H. Su, M. Huang, M. Ma, "DC Line Protection for Flexible MVDC Distribution Grid With Renewable Energy Resources", IEEE Power & Energy Society General Meeting (PESGM), Portland, USA, 2018, pp. 1-6, doi: 10.1109/PESGM.2018.8586429.
[12] Y. Li, V. Mohan, S. Jiang, Y. Wang and J. Liang, "Wavelet Transform based Differential Protection for MVDC Distribution Network," 2022 57th International Universities Power Engineering Conference (UPEC), Istanbul, Turkey, 2022, pp. 1-6, doi: 10.1109/UPEC55022.2022.9917599.
[13] M.J. Pérez-Molina, P. Eguia, D.M. Larruskain, E. Torres, O. Abarrategi, J.C. Sarmiento-Vintimilla, "Single-ended limiting inductor voltage-ratio-derivative protection scheme for VSC-HVDC grids", International Journal of Electrical Power & Energy Systems, Vol. 147, 2023, 108903.
[14] W. Leterme, N. Ahmed , J. Beerten, L. Ängquist , D. Van Hertem and S. Norrga, "A new HVDC grid test system for HVDC grid dynamics and protection studies in EMT-type software", IET International Conference on AC and DC Power Transmission, Birmingham, UK, 10-12 february 2015.
[15] V. Psaras, D. Tzelepis, D. Vozikis, G.P. Adam and G. Burt, "Non-Unit Protection for HVDC Grids: An Analytical Approach for Wavelet Transform-Based Schemes", IEEE Transaction on Power Delivery, Vol. 36, N. 5, October 2021.
[16] D.M. Larruskain, P. Eguia, A. Iturregi, E. Torres, V. Valverde and A. Blazquez, "Protection of DC grids with renewable energy sources and electrolyzers for green hydrogen production" ICREPQ'23, Madrid 2023.